Supporting Information

Direct Observation of Perovskite Photodetector Performance Enhancement by Atomically-Thin Interface Engineering

Zibo Li,[†] *Jieni Li,*[†] *Dong Ding,*[†] *Huizhen Yao,*[†] *Lai Liu,*[†] *Xue Gong,*[†] *Bingbing Tian,*[†] *Henan Li,*[‡] *Chenliang Su,*[†,§] *Yumeng Shi**[†,§]

[†] SZU-NUS Collaborative Innovation Center for Optoelectronic Science&Technology, International Collaborative Laboratory of 2D Materials for Optoelectronics Science and Technology of Ministry of Education, College of Optoelectronic Engineering, Shenzhen University, Shenzhen 518060, China.

[‡] College of Electronic Science and Technology, Shenzhen University, Shenzhen 518060, China.

[§] Engineering Technology Research Center for 2D Material Information Function Devices and Systems of Guangdong Province, College of Optoelectronic Engineering, Shenzhen University, Shenzhen 518060, China.

Corresponding author:
Yumeng Shi, E-mail: yumeng.shi@szu.edu.cn

Note S1. Definition of Richardson constant

The Richardson constant (A*) is expressed as follows: □

$$A^* = \frac{4\pi q m k_B^2}{h^3}$$

where k_B denotes the Boltzmann constant, q the electronic charge, m the electron mass, and h the Planck constant. [1,2]

Note S2. Estimation of effective contact area (A_e)

In our C-AFM experimental setup the nanoscale contacts are formed between the conductive tip and sample. We used the Hertz contact theory to estimate the effective contact area.[3,4] The tip is assumed to be an elastic sphere and the underlying sample surface is assumed to be flat to describe the contact formed between the tip and WS_2 nanosheets, as schematically illustrated in Figure S7a. Figure S7b shows the deformation image of $WS_2/MAPbI_3$ heterojunction, which can be used to extract the insert depth of tip. Figure S7c shows the AFM topographic image of RS-15M, which is very sharp to estimate tip's radius (r) at the insert depth. At last, the effective contact area was calculated as:

$$A_e = \pi r^2$$

~9.63 nm^2 for $WS_2/MAPbI_3$ and 6.54 nm^2 for $MAPbI_3$.

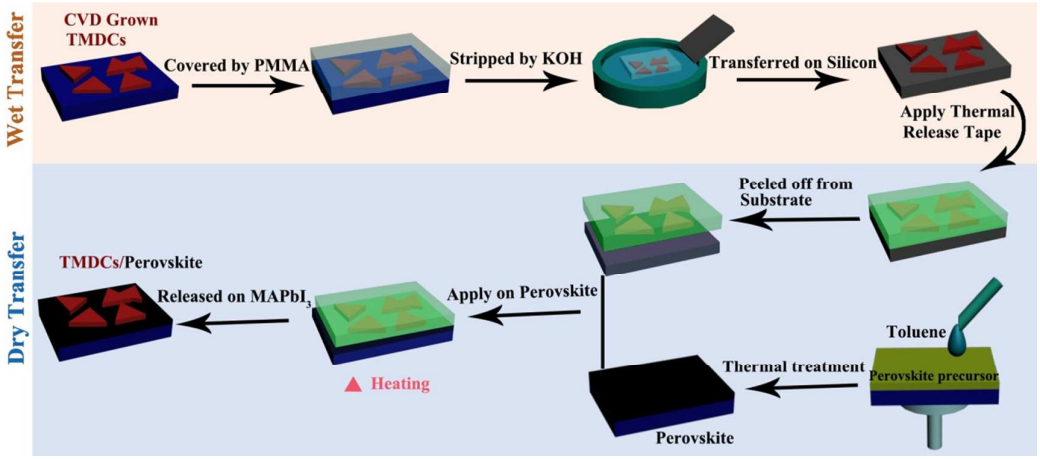

Figure S1. Schematic illustration of the fabrication process of $WS_2/MAPbI_3$ heterostructure.

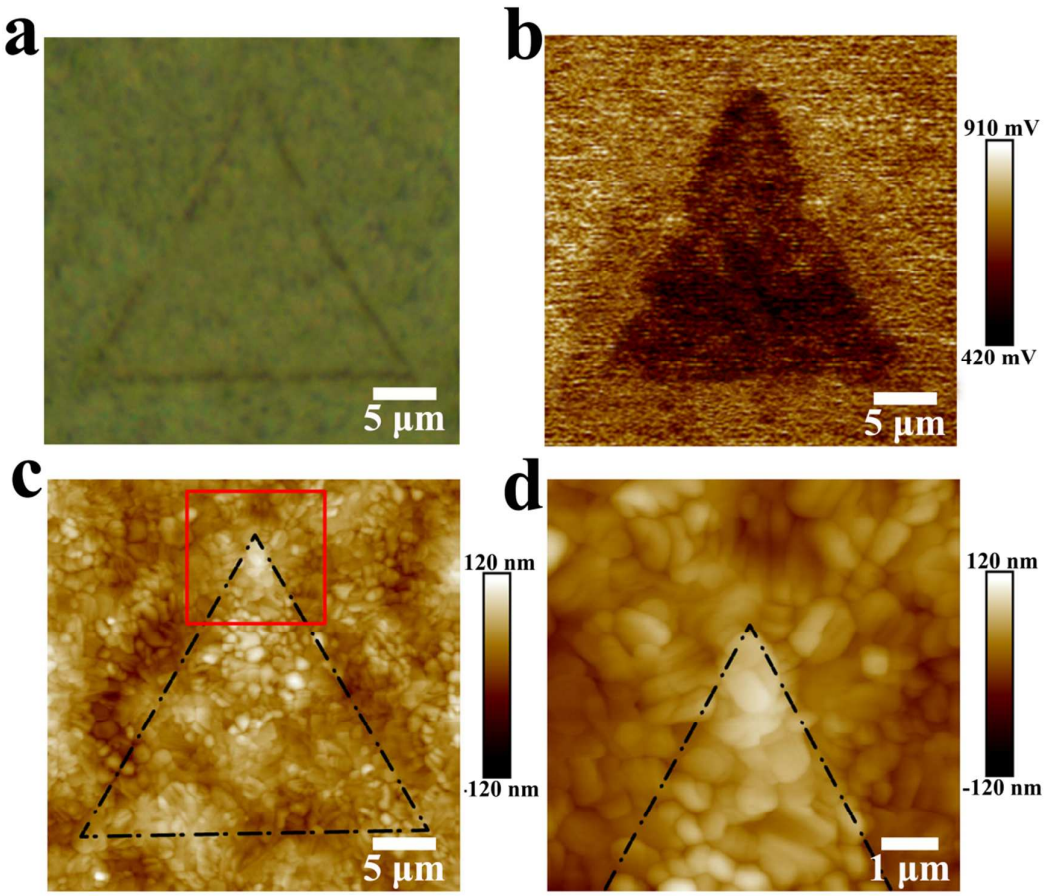

Figure S2. (a) Optical microscope image. **(b)** Surface potential image of $WS_2/MAPbI_3$ heterostructure. **(c)** AFM topographic image. **(d)** The zoom-in topographic image of the red frame in **(c)**.

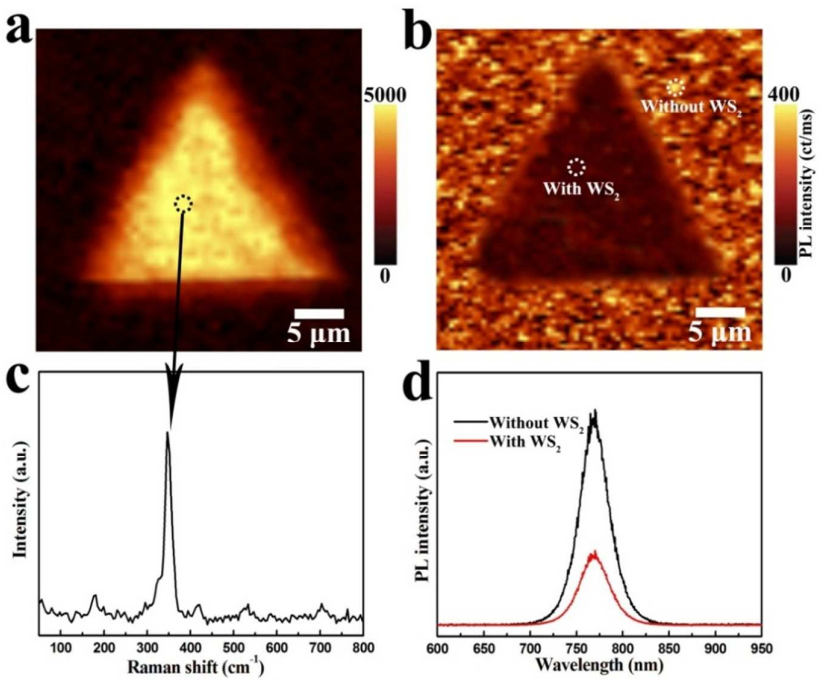

Figure S3. (a) Spatial distribution image of the Raman mapping of $WS_2/MAPbI_3$ heterostructure. **(b)** Spatial distribution image of the PL mapping of $WS_2/MAPbI_3$ heterostructure. **(c)** Raman spectra at the position as a circle marked in **(a)**. **(d)** PL spectra at the position as the circles marked in **(b)**.

The spatial distribution images of the Raman and PL intensity mapping of $WS_2/MAPbI_3$ heterostructure are shown in Figure S3. The Raman intensity distribution of 349 cm^{-1} peak from WS_2 layer in Figure S3a suggests the continuous distribution of WS_2 layer on perovskite surface without breaking. Additionally, the PL intensity mapping of perovskite exhibits relatively weak PL emission with a wavelength around 775 nm, when $MAPbI_3/WS_2$ heterostructure was formed. The PL quenching of the $MAPbI_3$ can be attributed to the interfacial charge transfer, which is also in good consistence with the results in Figure 1f.

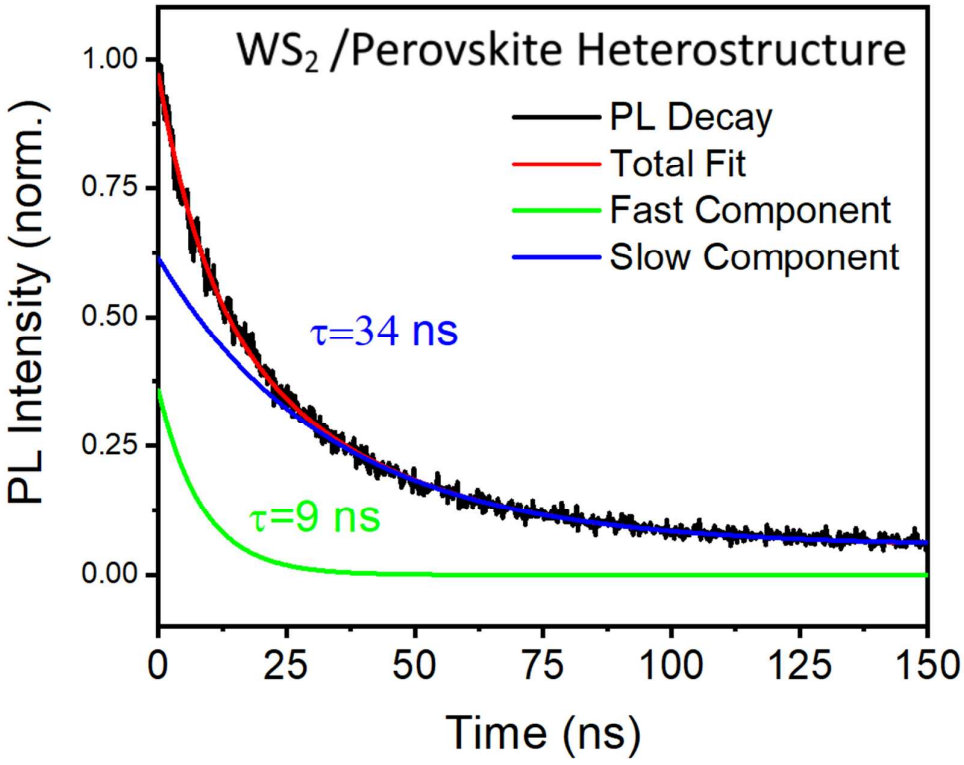

Figure S4. PL time decay trace on a WS_2/$MAPbI_3$ bilayer with biexponential fits showing a fast (t ≈ 9 ns) and a slow transient (t ≈ 34 ns).

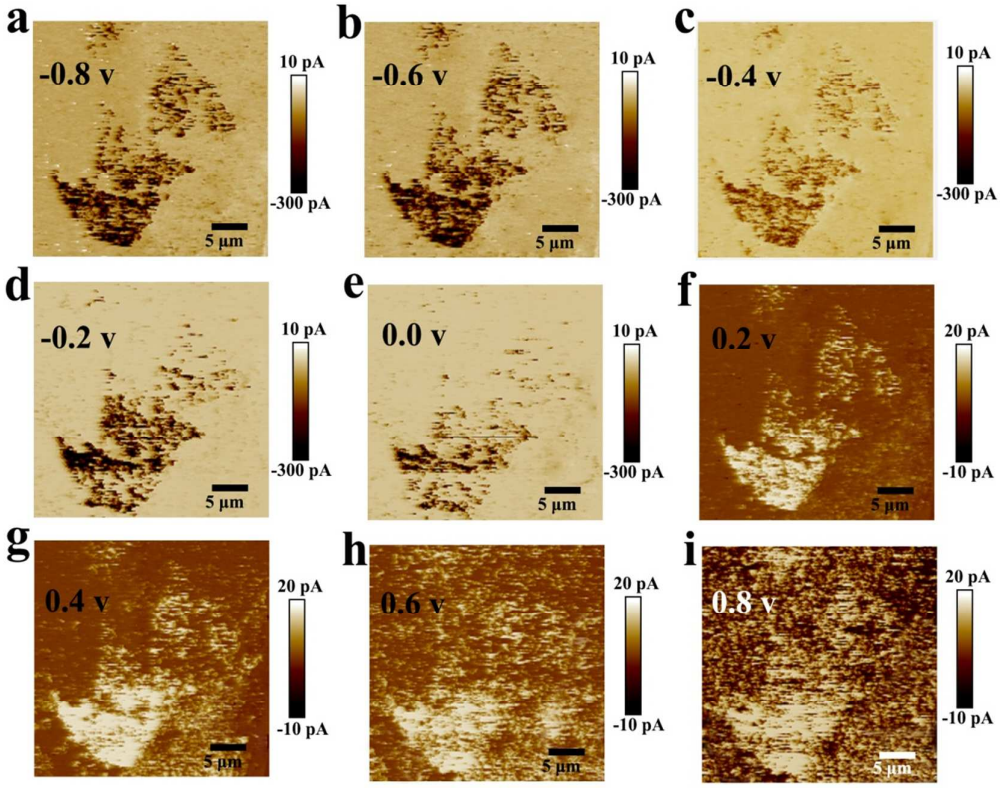

Figure S5. Current maps generated by conductive AFM measurements in dark with applied sample bias voltages of **(a)** -0.8 V, **(b)** -0.6 V, **(c)** -0.4 V, **(d)** -0.2 V, **(e)** 0.0 V, **(f)** 0.2 V, **(g)** 0.4 V, **(h)** 0.6 V, and **(i)** 0.8 V

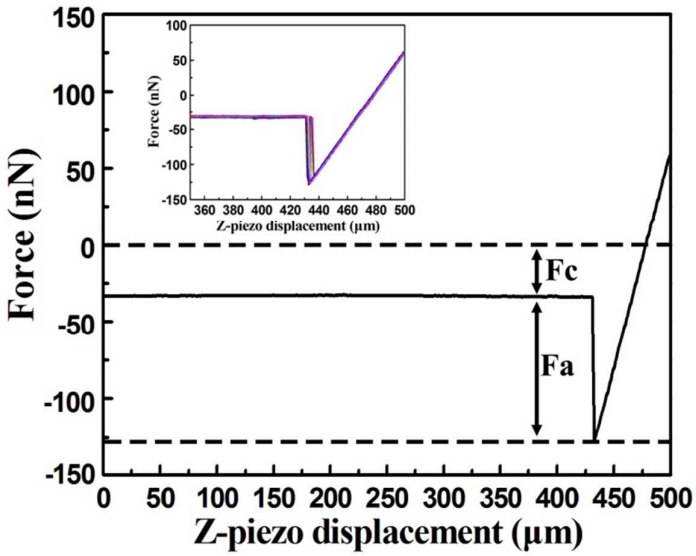

Figure S6. Representative force-displacement (F-D) curve in which F_c represents the instrumental deflection set-point force and F_a shows the additional force between the tip and the sample surface. Inset shows a series of F-D curves taken before and after each of the current images.

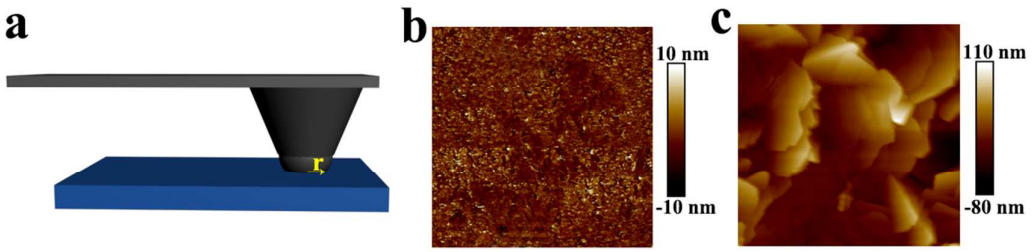

Figure S7. (a) Schematic illustration of the contact status between conductive tip and sample surface, r the contact area radius. **(b)** Deformation image of $WS_2/MAPbI_3$ heterojunction. **(c)** AFM topographic image of RS-15M.

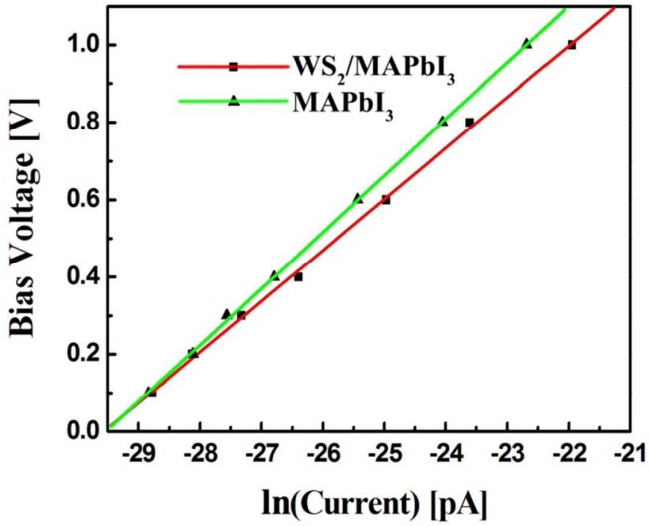

Figure S8. A semilogarithmic plot of bias voltage as a function of ln(current). The red and green straight lines indicate linear fit to the data.

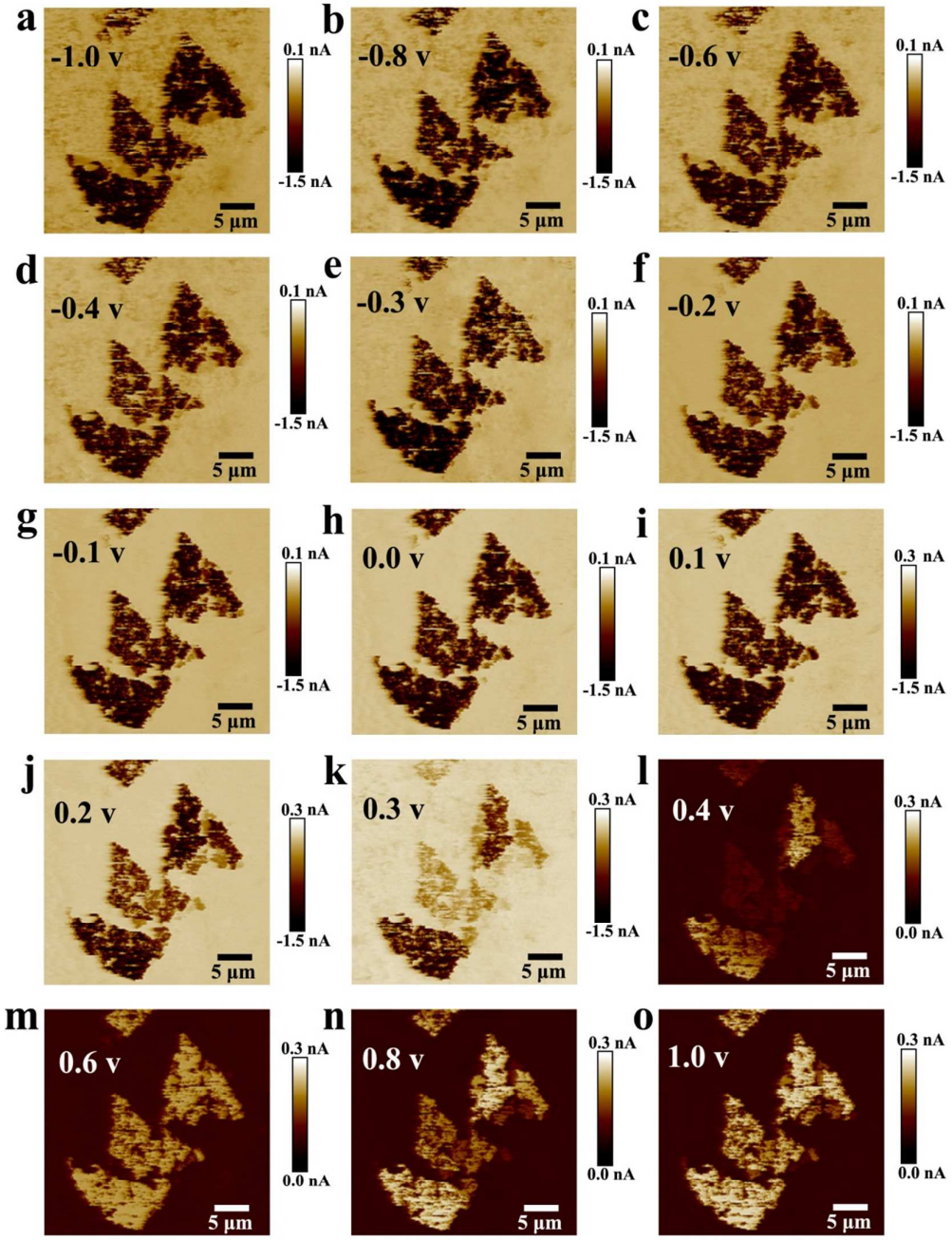

Figure S9. Current maps generated by PC-AFM measurements under laser illumination of λ=532 nm with applied sample bias voltages of **(a)** -1.0V, **(b)** -0.8 V, **(c)** -0.6 V, **(d)** -0.4 V, **(e)** -0.3 V, **(f)** -0.2 V, **(g)** -0.1 V, **(h)** 0.0 V, **(i)** 0.1 V, **(j)** 0.2 V, **(k)** 0.3 V, **(l)** 0.4 V, **(m)** 0.6 V, **(n)** 0.8 V and **(o)** 1.0 V.

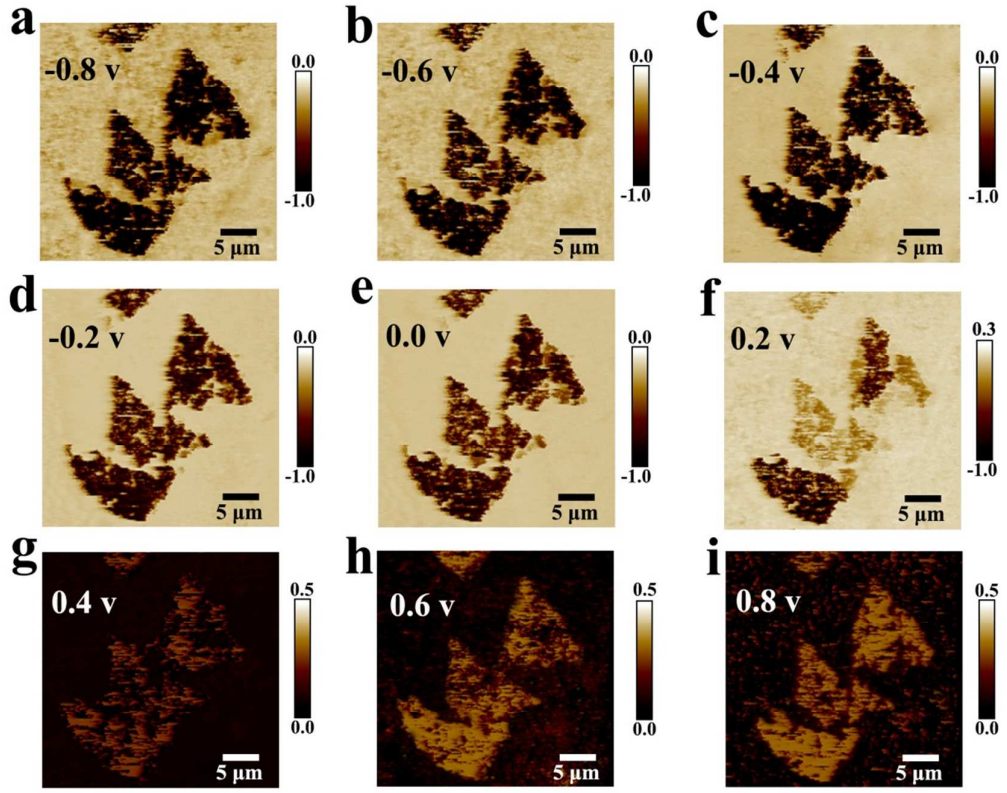

Figure S10. Photoresponse maps at applied sample bias voltages of **(a)** -0.8 V, **(b)** -0.6 V, **(c)** -0.4 V, **(d)** -0.2 V, **(e)** 0.0 V, **(f)** 0.2 V, **(g)** 0.4 V, **(h)** 0.6 V, and **(i)** 0.8 V under illumination of λ=532 nm.

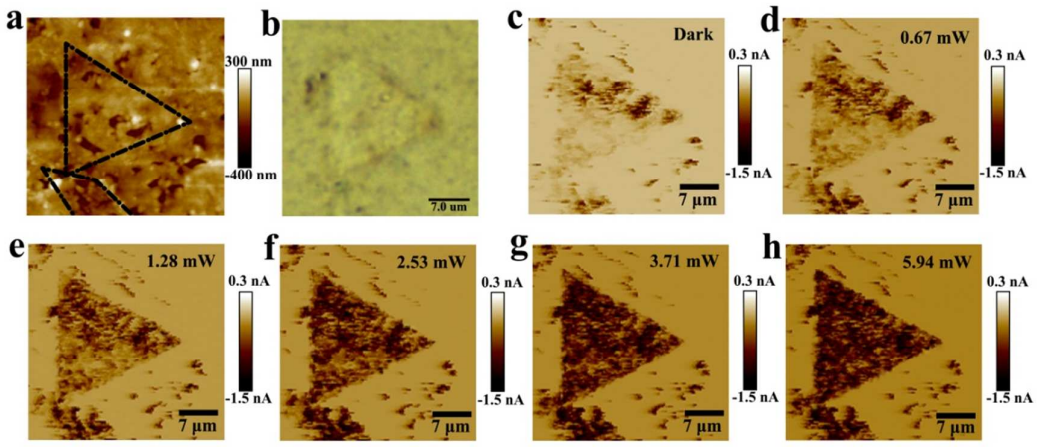

Figure S11. (a) AFM topographic image of the $WS_2/MAPbI_3$ heterojunction. **(b)** Optical microscope image of the $WS_2/MAPbI_3$ heterojunction. Photocurrent maps under varying incident laser power of **(c)** Dark **(d)** 0.67 mW, **(e)** 1.28 mW, **(f)** 2.53 mW, **(g)** 3.71 mW, **(h)** 5.94 mW under illumination of λ=532 nm, which are used to generate the photoresponse maps presented in Figure 6a-e in the main text.

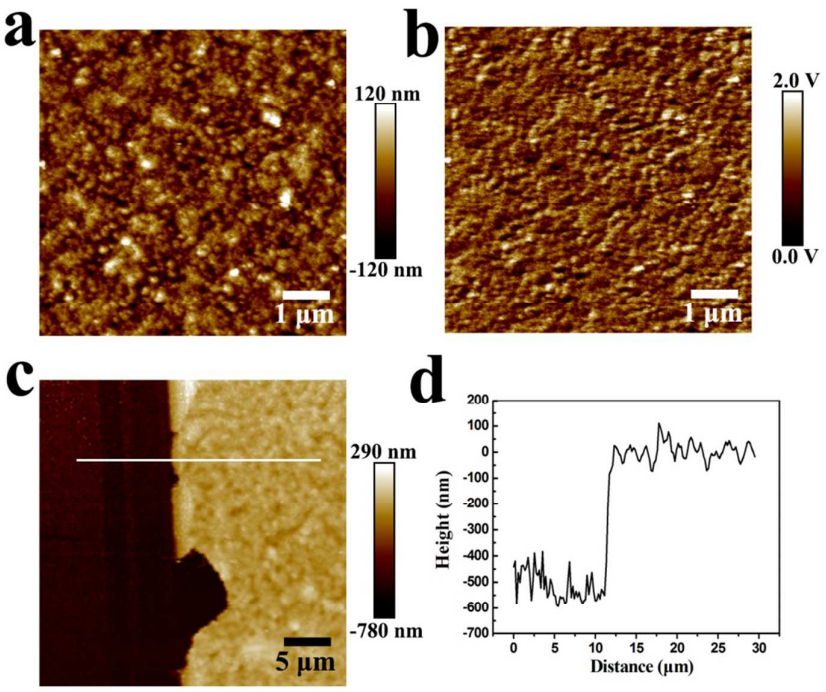

Figure S12. (a) AFM topographic image of perovskite film. **(b)** Surface potential image of the perovskite. **(c)** AFM topographic image of perovskite film, the darker region on the left is ITO substrate. **(d)** Height curve corresponding to the white line in panel c.

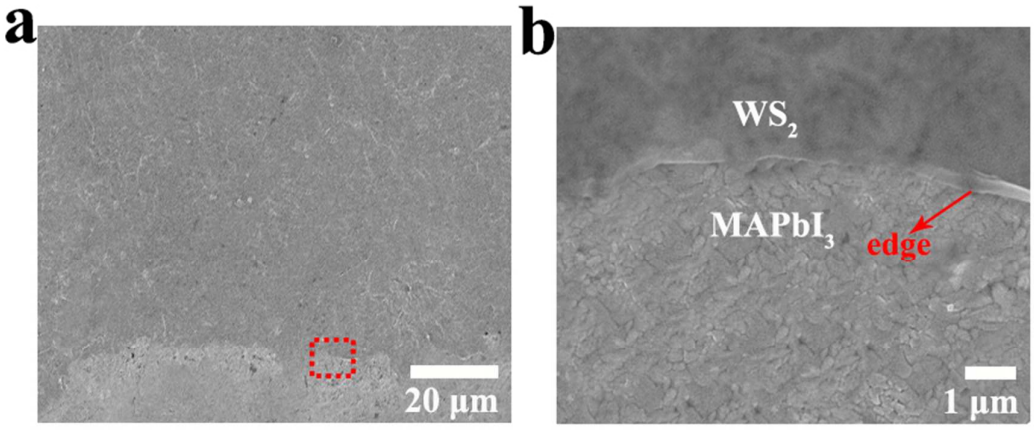

Figure S13. (a) SEM image of WS_2/$MAPbI_3$ junction. **(b)** The zoom-in topographic image of the red frame region in **(a).**

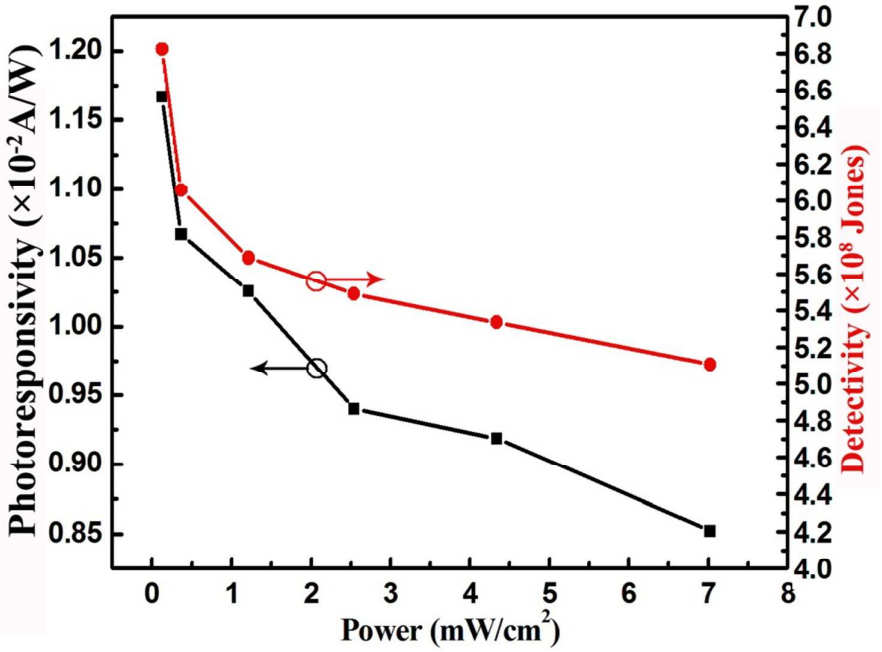

Figure S14. Photoresponsivity and detectivity of the $MAPbI_3$-only photodetector under -2.5 V.

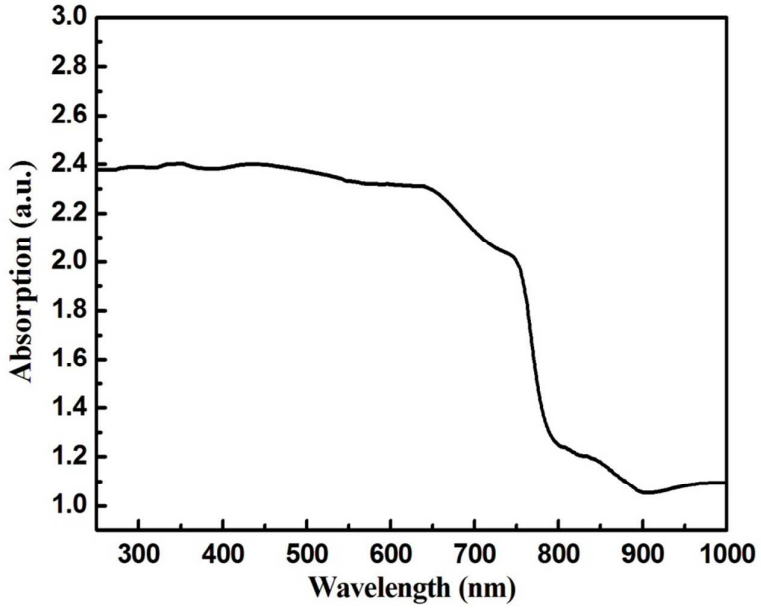

Figure S15. The absorption spectra of $WS_2/MAPbI_3$ junction.

REFERENCES

(1) Ruskell, T. G.; Workman, R. K.; Chen, D.; Sarid, D.; Dahl, S.; Gilbert, S. High Resolution Fowler-Nordheim Field Emission Maps of Thin Silicon Oxide Layers. *Appl. Phys. Lett.* **1996**, *68*, 93.

(2) Sze, S. M. *et al.* Physics of semiconductor devices. 3rd ed.; *Wiley-Interscience*: *Hoboken*, *NJ*, 2007.

(3) Cappella, B.; Dietler, G. Force-Distance Curves by Atomic Force Microscopy. *Surf. Sci. Rep.* **1999**, *34*, 1-104.

(4) Frammelsberger, W.; Benstetter, G.; Kiely, J.; Stamp, R. C-AFM-Based Thickness Determination of Thin and Ultra-Thin SiO_2 Films by Use of Different Conductive-Coated Probe Tips. *Appl. Surf. Sci.* **2007**, *253*, 3615-3626.